Highly durable anode supported solid oxide fuel cell with an infiltrated cathode

Alfred Junio Samson*, Per Hjalmarsson, Martin Søgaard, Johan Hjelm, Nikolaos Bonanos

Department of Energy Conversion and Storage, Technical University of Denmark, Risø Campus, Frederiksborgvej 399, DK-4000 Roskilde, Denmark

HIGHLIGHTS

► Electrochemically stable anode supported cell (ASC) with an LSC infiltrated-CGO cathode.
► No measurable degradation during 1500 h long operation at 700 °C and 0.5 A cm^{-2}.
► No change in impedance spectra recorded *in situ*.
► Post test characterization revealed no change in microstructure of the LSC infiltrate.
► ASC power density reached 0.79 W cm^{-2} at 750 °C at a cell voltage of 0.6 V.

ARTICLE INFO

ABSTRACT

An anode supported solid oxide fuel cell with an La$_{0.6}$Sr$_{0.4}$Co$_{1.05}$O$_{3-\delta}$ (LSC) infiltrated-Ce$_{0.9}$Gd$_{0.1}$O$_{1.95}$ (CGO) cathode that shows a stable performance has been developed. The cathode was prepared by screen printing a porous CGO backbone on top of a laminated and co-fired anode supported half cell, consisting of a Ni–yttria stabilized zirconia (YSZ) anode support, a Ni–scandia-doped yttria-stabilized zirconia (ScYSZ) anode, a ScYSZ electrolyte, and a CGO barrier layer. LSC was introduced into the CGO backbone by multiple infiltrations of an aqueous nitrate solution followed by firing. The cell was tested at 700 °C under a current density of 0.5 A cm^{-2} for 1500 h using air as oxidant and humidified hydrogen as fuel. The electrochemical performance of the cell was analyzed by impedance spectroscopy and current–voltage relationships. No measurable degradation in the cell voltage or increase in the resistance from the recorded impedance was observed during long term testing. The power density reached 0.79 W cm^{-2} at a cell voltage of 0.6 V at 750 °C. Post test analysis of the LSC infiltrated-CGO cathode by scanning electron microscopy revealed no significant micro-structural difference to that of a nominally identical untested counterpart.

© 2012 Elsevier B.V. All rights reserved.

1. Introduction

In recent years, the infiltration method has been a widely popular approach in preparing composite electrodes for use in solid oxide fuel cells (SOFCs). Many groups have reported exceptionally good anode and cathode performances obtained by incorporating nanoparticulate catalysts via infiltration (Refs. [1–3] and references therein). Cathodes have typically been prepared by infiltration with mixed ionic and electronic conductors such as lanthanum cobaltite-based perovskites into a ceria based backbone [4–6]. These cathodes have very low polarization resistance (R_p) and are especially promising candidates for use in low and intermediate temperature (500–700 °C) SOFCs. In terms of overall mechanical stability under thermal cycling, infiltrated cathodes appear to be more robust as the

thermal expansion coefficient (TEC) mismatch is overcome by forming a porous yet rigid and continuous backbone that is fired at high temperature followed by infiltration which forms nanoparticles only on the surface of the backbone. Delamination is also less likely to take place in this configuration as the backbone, which is fired at high temperatures, provides continuity with the electrolyte and is also usually TEC-matched with the half-cell. Despite these and the advantage of improved electrochemical performance over their conventionally prepared counterparts, the use of infiltrated cathodes in complete fuel cells is so far limited. As a consequence, so is the knowledge of the lifetime of infiltrated electrodes under long term operation. Possible reasons for not implementing this type of cathode in SOFCs are among others: (i) the need for multiple number of infiltrations to achieve the desired amount of electrocatalysts, and (ii) the perceived instability of nanoparticulate infiltrates during long term operation. Specifically, the high surface area-nanoparticles are highly prone to coarsening and grain growth which increase R_p.

Studies on long term stability of infiltrated cathodes have been very limited to date despite its importance for the application of fuel cell technology. The problem of coarsening in an infiltrated cathode has been demonstrated by Wang et al. [7] on a cathode consisting of $La_{0.8}Sr_{0.2}FeO_{3-\delta}$ (LSF) infiltrated into an yttria-stabilized zirconia (YSZ) backbone, where a symmetrical cell fired at 850 °C shows a linear increase in R_p from 0.15 to 0.55 Ω cm^2 after testing for 2500 h at 700 °C. SEM observations on a recent study from our group on $La_{0.6}Sr_{0.4}Co_{1.05}O_{3-\delta}$ (LSC) infiltrated − $Ce_{0.9}Gd_{0.1}O_{1.95}$ (CGO) symmetrical cathodes also demonstrated a certain degree of particle coarsening depending on the maximum infiltrate firing temperature and operation time [6]. In other studies, however, it appears that other infiltrated cathodes possess a high degree of stability for long term operation. For example, no increase in R_p was observed for an LSC infiltrated − $Sm_{0.2}Ce_{0.8}O_{1.9}$ (SDC) symmetrical cathode upon thermal cycling and holding at 600 °C for 2000 h [5]. However, the R_p obtained in the aforementioned study was already fairly high (0.3 Ω cm^2) from the beginning of the test where the electrode was fired at maximum temperature of 800 °C. High stability was also reported for a cathode with $La_{0.85}Sr_{0.15}MnO_3$ (LSM) infiltrated into scandia stabilized zirconia (SSZ) and fired at a maximum temperature of 900 °C. The infiltrated cathode with Ni−SSZ anode and SSZ as electrolyte showed no significant changes in the electrochemical performance or microstructure after testing for 500 h at 650 °C under a relatively low, near-constant applied current of 0.15 A cm^{-2} [8]. Long term stability of infiltrated cathodes is still an open issue and requires a more comprehensive study to understand the effects of several factors such as the operating temperature, infiltrate firing temperature, and infiltrate−backbone combination. Another important consideration is on how these infiltrated cathodes perform when integrated onto an actual SOFC and tested under high current densities.

In our previous work, we have presented, based on symmetrical cell measurements, an exceptional initial performance of an LSC infiltrated-CGO cathode (0.044 Ω cm^2 at 600 °C) [6]. The infiltrated cathode also showed satisfactory stability during long term operation, with R_p leveling out at 0.07 from 0.04 Ω cm^2 after 450 h at 600 °C [6]. In this work, such a cathode has been integrated onto an anode supported, thin electrolyte SOFC and tested for long term stability. The anode supported half cell consists of a Ni−YSZ anode support, a Ni−ScYSZ anode, where ScYSZ is 10 mol% Sc_2O_3, 1 mol% Y_2O_3-stabilized ZrO_2, a ScYSZ electrolyte, and a $Ce_{0.9}Gd_{0.1}O_{1.95}$ (CGO) barrier layer. A schematic of the cross section of the cell is shown in Fig. 1. A long term test running over 1500 h under constant operating conditions was performed on the cell. Scanning electron microscopy was employed to analyze the resulting microstructures of the infiltrated cathode after long term testing. The electronic conductivity of the infiltrated cathode was also investigated to estimate the extent of its contribution to the electronic ohmic loss in the cell.

2. Experimental

The electronic conductivity of the infiltrated cathode in a symmetrical cell configuration was studied as a function of LSC loading and LSC firing temperature. Backbones of $Ce_{0.9}Gd_{0.1}O_{1.95}$ (CGO) were applied by screen printing an in-house prepared CGO ink onto both sides of a 5 × 5 cm^2, dense 180 µm thick CGO electrolyte (KERAFOL). The sample was fired at 1050 °C for 2 h, resulting in a backbone with a thickness of about 25 µm. Samples with approximate size of 6 × 6 mm^2 were cut from the large symmetric cell and were subsequently infiltrated 6, 9, and 12 times with a precursor solution of metal nitrates corresponding to the nominal composition $La_{0.6}Sr_{0.4}Co_{1.05}O_{3-\delta}$. The LSC precursor
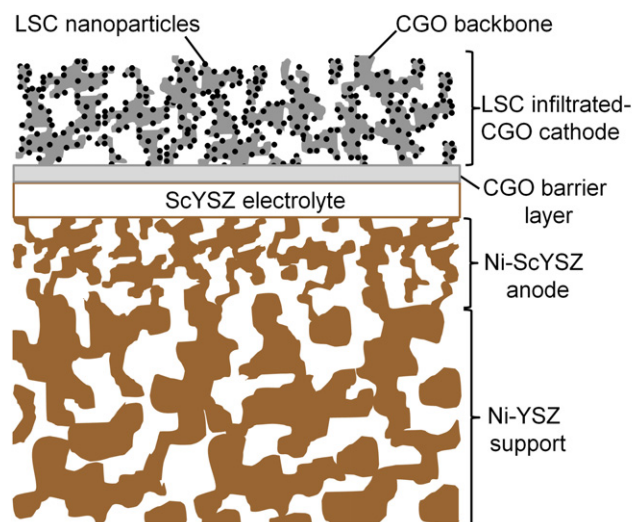

Fig. 1. Schematic of the anode supported cell used in the study. The relative thicknesses and microstructures are not drawn to scale.

solution for infiltration was prepared such that it would contain 0.1 mol of the nominal composition $La_{0.6}Sr_{0.4}Co_{1.05}O_{3-\delta}$ after calcination. The final volume of the precursor solution was fixed to 100 mL after partial evaporation of water. Correspondingly, the La:Sr:Co mol ratio in the precursor solution was 0.06:0.04:0.105. The precursor solution preparation and the infiltration methodology have already been described in our previous work [6]. The final volume fraction of the infiltrated material after 6, 9, and 12 times infiltration are 12, 17, and 19 vol% out of the total volume of the cathode. The estimation of the amount of infiltrated material and the appearances of the infiltrated structure before and after infiltration, including the effects of the firing temperature are also described in our previous work [6].

The in-plane electrical conductivity was measured using a 4-probe direct-current (DC) method. A schematic of the setup for one symmetric cell is shown in Fig. 2a. Platinum wires were wound near the end sides of the sample and additionally painted with Pt paste to ensure a negligible contact resistance of the wire to the infiltrated cathode. Current is passed through the sample and the voltage drop is measured across a distance, l, in the middle of the sample. The samples are placed in series together with a 1 Ω resistor to monitor the current, as shown in Fig. 2b. The resistance obtained (R_{eq}) corresponds to that of the two cathodes in parallel. Although the electrolyte and porous backbone also carry some of the current in the form of oxide ions, this is estimated to be much smaller than that carried by the cathodes. This can be argued from the fact that the measured R_{eq}'s are significantly smaller than that of the resistance calculated for a dense CGO using literature values for its conductivity [9] (e.g. R_{eq} = 11.5 Ω and $R_{dense\ CGO}$ = 1000 Ω at 600 °C, 6× infiltration) and the dimensions in the experiment. The R_{eq}'s from each of the samples are calculated from the measured current running through the circuit and the voltage drops from each sample. The conductivity at each LSC firing temperature (T_{max}) is then calculated using the equation, $\sigma = l/RA$, where A is the cross-sectional area of the infiltrated cathode, and $R = 2R_{eq}$.

A 53 mm × 53 mm large anode supported half cell that consisted of a Ni−YSZ support/Ni−ScYSZ anode/ScYSZ electrolyte/CGO barrier layer was manufactured by tape-casting and lamination and co-fired above 1200 °C. Before screen printing the CGO backbone, a CGO precursor solution was spin coated on top of the CGO barrier layer and fired at 350 °C to further enhance the connectivity of the
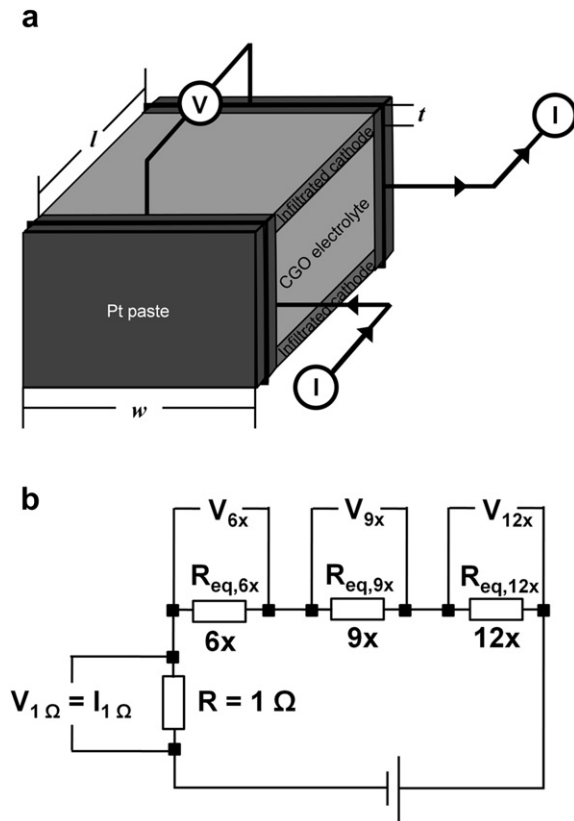
a

b

Fig. 2. (a) Schematic of the in-plane conductivity measurement setup for one symmetric cell. (b) The equivalent circuit used to measure the in-plane conductivity of the three symmetric cells (labeled 6×, 9×, and 12×). Voltage drops, V_{nx}, are recorded for each sample as a function of the LSC firing temperature.

barrier layer and the CGO backbone. To integrate the infiltrated cathode, an in-house $Ce_{0.9}Gd_{0.1}O_{1.95}$ (CGO) ink was screen printed onto the half cell and fired at 1050 °C for 2 h to serve as a backbone. The backbone was subsequently infiltrated nine times with a precursor solution of metal nitrates corresponding to the nominal composition $La_{0.6}Sr_{0.4}Co_{1.05}O_{3-\delta}$.

The cell was tested in a SOFC test setup described elsewhere [10]. Custom glass sealant frames with glass softening and glass transition temperatures of approximately 670 °C and 790 °C, respectively, were used to seal the anode and cathode gas flow compartments. Gold and nickel meshes were used as current collector components on the cathode and anode side, respectively. Eight kilograms of weight was applied on top of the cell house to ensure gas tight sealants and electrical contact. The flow compartments were sealed at 850 °C for 2 h prior to anode reduction in 9% H_2 in N_2 for 2 h and 4% H_2O in H_2 for 1 h. The cell was tested starting from 850 °C down to 650 °C with 50 °C increments using $i-v$ polarization and electrochemical impedance spectroscopy (EIS) measurements. The stability of the cell was investigated in a galvanostatic durability experiment carried out at 700 °C and 0.5 A cm^{-2} with fuel and oxygen utilization of 60% and 20% respectively. The cell was also characterized under different partial pressure of oxygen on the cathode side and partial pressure of H_2O on the anode side.

Post-test micro-structural analysis was carried out using a Zeiss Supra-35 scanning electron microscope on the infiltrated cathode and cell and on a nominally identical counterpart. The counterpart had been heated to 850 °C for 6 h in air at a heating rate of 60 °C h^{-1} in order to prepare a sample that is representative of a not long term tested SOFC.

3. Results and discussion

3.1. Electrical conductivity of LSC infiltrated-CGO cathodes

Shown in Fig. 3 is the dependence of the total conductivity of the symmetric cells at 600 °C with the number of LSC infiltrations and maximum LSC firing, T_{max}. It is important to point out that the "LSC" infiltrate in this study is multi-phased as seen in a recent study from our group [6]. Hence, in reality the calculated conductivity originates from a mixture of these phases. The infiltrate will in the following be called "LSC" even though it is known to be multi-phased. It should also be noted that polished cross sections (not shown) of the samples infiltrated 9 and 12 times reveal a porous LSC residue layer with thicknesses between 500 nm and 1 μm on top of the LSC infiltrated-CGO backbone. In principle, the residue layer may interfere with the measurement of the in-plane electronic conductivity especially if the infiltrate has a very high electronic conductivity. Thus, the measured in-plane conductivity values for these samples will only be treated as maximum values. As the 6× infiltrated sample appear not to have a residue layer, the measured in-plane conductivity values for this sample will serve as a minimum for the 9 and 12× infiltrated samples. In practice, removing only the residue layer by polishing poses a challenge as it is difficult to ascertain that the infiltrated porous backbone has also not been removed.

From Fig. 3, it is clear that the conductivity increases with an increasing number of infiltrations irrespective of T_{max}. This is most probably due to increasing connectivity among the LSC nanoparticles as the LSC loading is increased. For all the infiltrations, it is observed that the increase in T_{max} from 600 to 900 °C causes a decrease in the total conductivity. For the 6× infiltrated sample, it has been shown in our previous study that the increase in T_{max} above 600 °C causes grain growth and coarsening [6]. Thus, the trend observed in Fig. 3 for the 6× infiltrated sample is most probably due to a loss of percolation due to grain growth and coarsening. For the 9× and 12× infiltrated samples, it was postulated in Ref. [6] that the loss of percolation due to grain growth and coarsening with increasing LSC firing temperature is not a problem. Thus it is expected that the conductivity would remain almost constant or, as was suggested by the decrease in R_s in Ref. [6] for these samples, the conductivity would increase with increasing firing temperature. As this is clearly not the case in Fig. 3, other factors have to be considered.
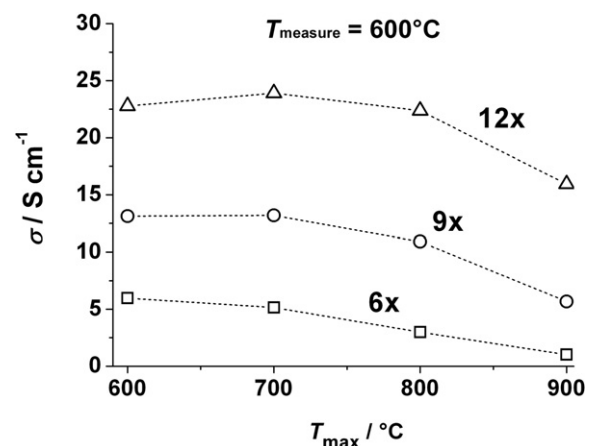

Fig. 3. Dependence of the total conductivity of the LSC infiltrated cathodes with number of infiltrations and maximum firing temperature, T_{max}.

From the conductivity values, it is possible to estimate the ohmic loss contribution of the LSC-infiltrated cathode if it is integrated to an anode supported SOFC. The number of infiltrations used in this study is fixed to nine times as this produces the lowest R_p's [6]. Assuming that the conductivity is comparable to that of a 6× infiltrated sample and is isotropic, the ohmic loss contribution at 600 °C for a 35 μm thick cathode and infiltrated 6× with LSC is only 0.59–3.4 mΩ cm^2 depending on T_{max}. For comparison, the ohmic loss from the combined thicknesses of the ScYSZ electrolyte and the CGO barrier layer based on SEM images is 112 mΩ cm^2 at 600 °C. Thus, it appears that the electronic conductivity of the infiltrated cathode will not limit the performance of a common anode supported SOFC in terms of electronic ohmic loss, provided that proper current collection on the cathode side is in place.

3.2. Cell performance and degradation

Fig. 4a shows the impedance at open circuit voltage (OCV) of the anode supported cell (ASC) at 650, 700 and 750 °C after heating the cell at 850 °C. For comparison, the impedance spectra of

a nominally identical cathode at OCV measured on a symmetric cell [6] at 700 °C is also shown in Fig. 4b. There were no impedance spectra at 650 and 750 °C collected for the symmetric cell. Note that in this case, the symmetric cell was fired at $T_{max} = 900$ °C. The serial resistance, R_s, which mainly originates from the 180 μm CGO electrolyte was subtracted from the impedance to focus only on R_p. It is seen that the R_p of the symmetric cell is 0.05 Ω cm^2. It is expected that the R_p for the symmetric cell will be slightly lower had it been fired at 850 °C as seen from relationships of R_p and T_{max} in our previous study [6]. The impedance spectra of the ASC at 700 °C in Fig. 4a indicate a total area specific resistance (ASR) of 0.73 Ω cm^2. From the thickness of the ScYSZ electrolyte estimated from SEM images and the ionic conductivity data of ScYSZ [11], the electrolyte ohmic loss contribution to the total ASR is 0.028 Ω cm^2 at 700 °C. The other major contributor to the ohmic losses is most probably the CGO barrier layer. In general, the number of components and interfaces in an ASC and the factors during its operation make it difficult to precisely distribute the ohmic loss contributions. What is clear, as pointed out in the conductivity calculations, is that the ohmic loss contribution of the LSC infiltrated cathode is not significant. Although the data are not sufficient to ascertain the polarization loss contributions of each of the electrodes, it is clear from Fig. 4 that the impedance contribution of the infiltrated cathode is probably not above 7% out of the total impedance of the cell. Fig. 4c shows a comparison of the impedance spectra of the ASC with LSC infiltrated-CGO cathode and an ASC with a screen printed LSC–CGO (50:50 wt%, fired at 1000 °C in air) composite cathode at 750 °C. The two cells have identical electrolyte, anode, and anode support. It is clear that the ASC with LSC infiltrated-CGO cathode exhibits a higher ASR. It is not clear why this is the case, considering that in symmetrical cell testing, the LSC infiltrated cathode fired at a maximum 900 °C show comparable R_p's with that of screen printed LSC–CGO (50:50 wt%, fired at 1050 °C in air) composite cathode at high temperatures (>600 °C). This is shown in Fig. 5. The lower activation energy of the LSC infiltrated-CGO cathode is associated to a larger amount of CGO phase compared to the LSC–CGO composite cathode. CGO has lower activation energy for oxide ion conduction than LSC, as suggested by oxygen tracer diffusion experiments (LSC, 176 kJ mol^{-1} [12] and CGO, 87 kJ mol^{-1} [13]). Future studies involving low temperature maximum firing temperature for the LSC infiltrate and low temperature operation, where it is found to have lower R_p's than a conventional LSC–CGO
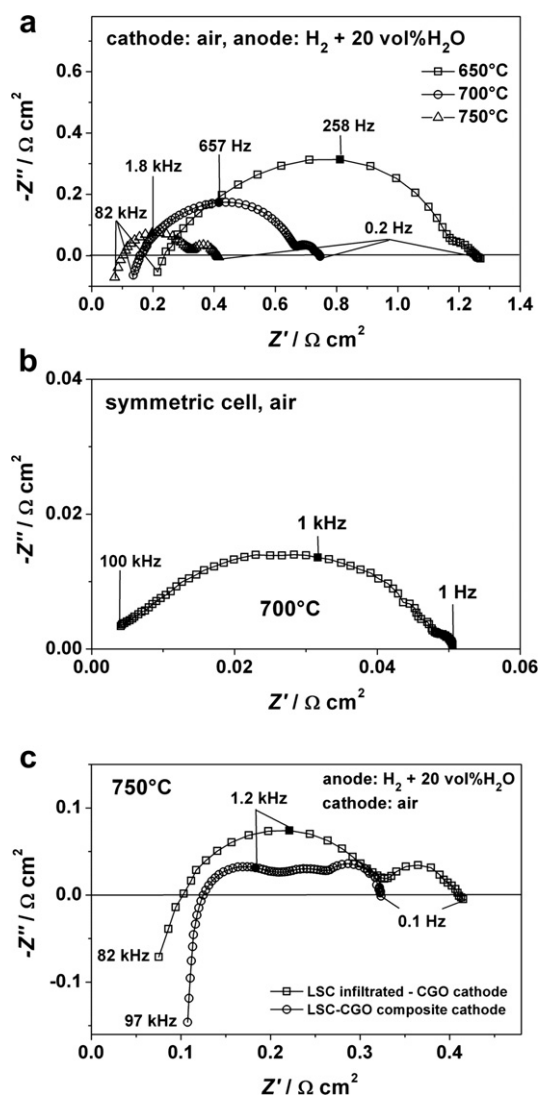
Fig. 4. Impedance spectra at OCV. (a) ASC at 650, 700 and 750 °C. (b) Symmetric cell with LSC-infiltrated cathode at 700 °C. (c) ASC with LSC infiltrated-CGO cathode compared to an identical ASC with screen printed LSC–CGO cathode at 750 °C.
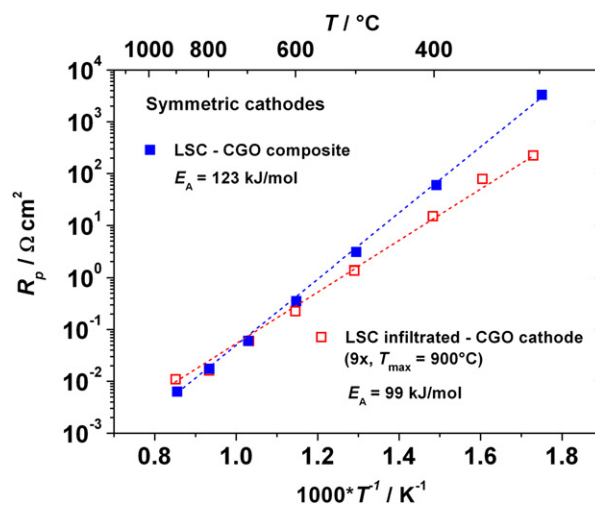
Fig. 5. R_p as a function of the reciprocal absolute temperature for an LSC–CGO composite cathode and an LSC infiltrated-CGO cathode. The number of infiltrations is 9× and the LSC infiltrate is fired at 900 °C.

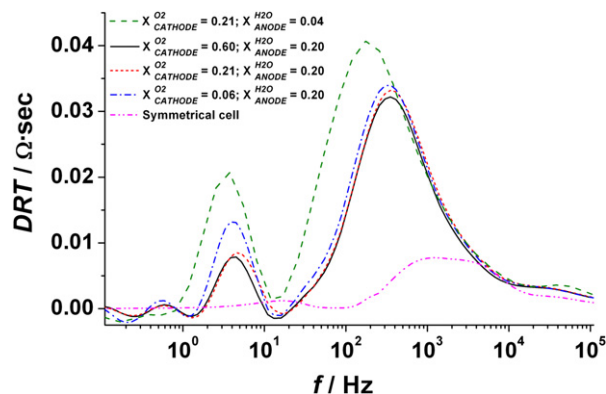**Fig. 6.** DRT analysis of the impedance measured at OCV after 1500 h testing at 700 °C for different cathode p_{O_2} and anode p_{H_2O}.

Fig. 8. Impedance spectra during testing at 700 °C under constant applied current of 0.5 A cm^{-2}. Impedance spectra recorded at selected times are shown.

composite cathode, and extended long term testing involving thermal cycling could provide a more comprehensive assessment of the advantages and disadvantages of LSC infiltrated cathodes.

The comparatively small contribution of the infiltrated cathode to the overall R_p can also be seen in the distribution of relaxation times (DRT) analysis of the cell as shown Fig. 6 for different oxygen and fuel partial pressures on the cathode and anode side, respectively, at 700 °C. A DRT analysis of a symmetric LSC infiltrated-CGO cathode is also shown for comparison. The impedance response is seen to consist of two main regions in different frequency ranges, 100–1000 Hz and 1–10 Hz. The region 1–10 Hz can be attributed to conversion and gas diffusion in both the anode and cathode side. This response is not related to the electrochemical characteristics of the cell and will, therefore not be discussed further in this paper. The main interest is the major impedance response at 100–1000 Hz. No considerable shift in this response is seen when the p_{O_2} in the cathode side is changed from 0.06 to 0.6 atm. However, when the p_{H_2O} is lowered from 0.20 to 0.04 atm while keeping the p_{O_2} in the cathode side to 0.21 atm, a shift in peak frequency and magnitude is observed. This suggests that the major contributor to the R_p in the range 100–1000 Hz is related to the anode. This agrees well with the comparatively low resistance for this type of cathode when measured in a symmetrical cell configuration.

Fig. 7 shows the cell voltage of the ASC, recorded at a constant applied current density of 0.5 A cm^{-2} for 1500 h at 700 °C. This long term galvanostatic test was started after an initial characterization of the cell, which means that the infiltrated cathode has been heated to 850 °C for several hours. It is evident from Fig. 7 that the
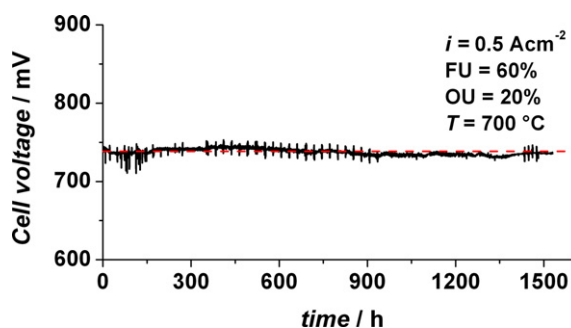
cell exhibits excellent stability with no measurable loss in cell voltage over 1500 h. The stability is also evident in Fig. 8 showing no measurable change in the impedance recorded *in situ* during the test. Also, from Fig. 8, it is obvious that no noticeable changes in both the serial resistance, R_s, and polarization resistance, R_p, can be observed. The impedance spectra in Fig. 8 indicate a total area specific resistance (ASR) of 0.52 Ω cm^2. A separate characterization of the processes found in both electrodes, especially the anode, under constant current using model cells, i.e., three-electrode or two electrode symmetric cell setups has not been performed. This makes the deconvolution of processes in the cell, and hence the quantitative identification of the contribution of each of the electrodes to the polarization resistance, very challenging. However, as explained earlier, symmetric cell characterizations of the LSC infiltrated cathode at OCV indicates that the cathode contribution to the overall R_p does not exceed 10%. This approximation assumes that the cathode impedance does not increase under current loading. There is reason to believe that this as a recent study on the current-static, cathodic polarization behavior of an LSC electrode on a samaria-doped ceria electrolyte does not yield any considerable effect on the performance of the LSC electrode [14]. It is clear from Figs. 7 and 8 that no significant degradation of the infiltrated cathode has occurred. The results also indicate stability of the other cell components.

Shown in Fig. 9 are the *i–v* and power characteristics at 750 °C of the ASC after long term testing. Similar data for an ASC with screen printed LSC–CGO cathode and nominally identical anode half cell is

Fig. 7. Cell voltage as function of operating time at 700 °C under a constant applied current of 0.5 A cm^{-2}. The dotted line indicates the cell voltage at the start of the test. The fuel utilization (FU) is adjusted to 60% on the anode side and 20% oxygen utilization (OU) on the cathode side. Spikes indicate impedance measurements.
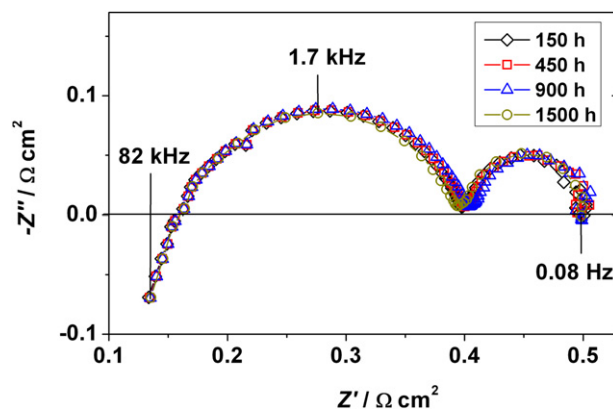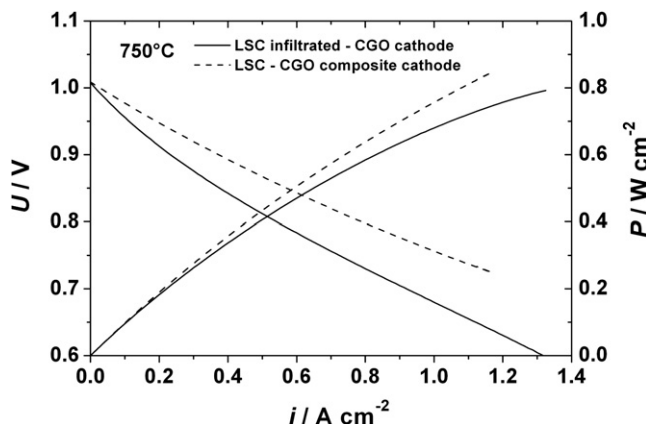

Fig. 9. Current–voltage and power curves for the anode supported cell with LSC infiltrated-CGO cathode and LSC–CGO composite cathode at 750 °C.
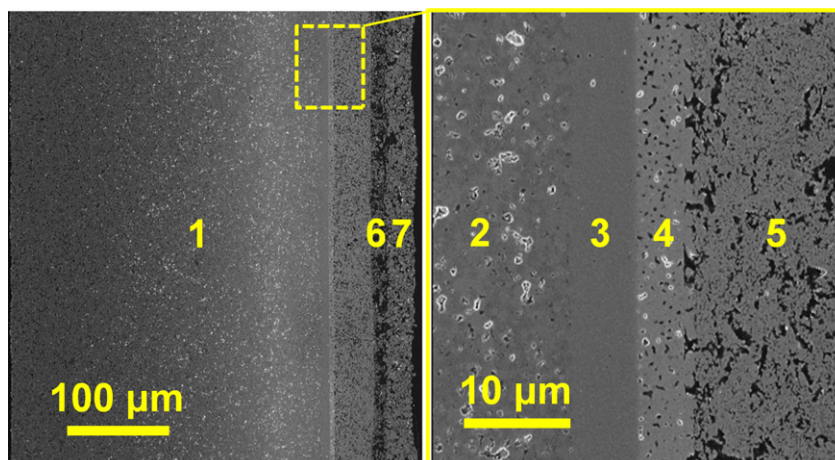
Fig. 10. Post mortem SEM micrographs of the cross section of the cell. A magnified image showing the anode, electrolyte, CGO barrier layer, and cathode is also shown. 1 − Ni–YSZ anode support, 2 − Ni–ScYSZ anode, 3 − ScYSZ electrolyte, 4 − CGO barrier layer, 5 − LSC infiltrated-CGO cathode, 6 − LSC residue layer, and 7 − Sr-doped lanthanum manganite (LSM) current collector.

also shown for comparison. The power density of the ASC with LSC infiltrated-CGO cathode reached 0.79 W cm^{-2} at 750 °C at a cell voltage of 0.6 V. The ASC with LSC–CGO composite cathode is clearly superior in terms of power characteristics, but as mentioned previously, more studies are required to assess the advantages of an LSC-infiltrated cathode.

3.3. Post test cell characterization

The SEM micrographs in Fig. 10 provide an overview of the cross section of the cell after long term testing. The magnified image shows in greater detail the anode, electrolyte, and cathode interfacial regions. No sign of significant micro-structural damage such as cracks are observed in any of the components. Another noticeable feature is the layer between the infiltrated cathode and the Sr-doped lanthanum manganite (LSM) current collector. This layer is composed of LSC that has not been completely infiltrated into the porous CGO backbone. Clearly, this residue layer, which is about 15 μm is much thicker than what is usually obtained for a symmetric cell as discussed previously (500 nm−1 μm). The much larger area of the CGO backbone in the ASC collects much more residue and is harder to remove than in the symmetric cell case. The microstructure, electrochemical performance, and in-plane electronic conductivity of this LSC residue layer has been investigated and the results are shown in the Supplementary Information. It is found that this layer can, in itself function as a cathode with an $R_p = 0.19$ Ω cm^2 at 600 °C in air when fired at 600 °C. However, as

the firing temperature is increased, the R_p drastically increases ($T_{max} = 900$ °C, 10.5 Ω cm^2 at 600 °C), which is most probably due to a decreasing surface area for oxygen surface exchange as the layer starts to densify. It is not difficult to see that the presence of a CGO backbone is important as it not only spreads the active surface but also provides a support to the LSC infiltrate which can limit the grain growth and densification of the infiltrate. One important role of the CGO backbone is that, due to its lower activation energy than LSC, the R_p for an LSC infiltrated-CGO cathode does not drastically increase with decreasing temperature (see Fig. S4 in the Supplementary Information). This makes the composite structure a much more feasible choice for operation at low temperatures.

Regarding electronic conductivity, it was found that the layer has a very high effective in-plane electronic conductivity (see Fig. S2 in the Supplementary Information). Thus, the LSC residue layer seen in Fig. 10 could have not possibly limited the transport of electrons from the current collector to the LSC infiltrated-CGO cathode. Poor electronic conduction could have led to a significantly higher ohmic loss.

Fig. 11 shows the SEM micrographs of the infiltrated cathode before and after long term test. The LSC phase is seen as interconnected particles of approximately 50–100 nm in size, coating the larger (∼200 nm) CGO particles. Several regions were examined in both cases but as seen in Fig. 11b, the microstructure of the infiltrated cathode after 1500 h of testing did not change in a clear visible way. Thus, it appears that the firing (during testing) performed at 850 °C was sufficiently high to induce a relatively stable
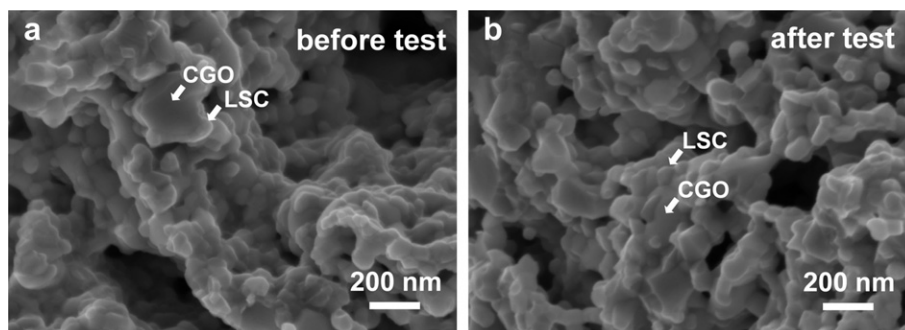

Fig. 11. SEM micrographs of the LSC infiltrated-CGO cathode (a) before and (b) after testing for 1500 h at 700 °C under constant applied current of 0.5 A cm^{-2}. CGO and LSC particles are identified.

LSC particle size and microstructure suited for a lower operating temperature (700 °C) even for a prolonged period of operation. These results are consistent with the very stable electrochemical performance measured on the ASC.

4. Conclusion

An anode supported cell with an LSC infiltrated-CGO cathode has been developed which showed high electrochemical stability. The cell was found to be electrochemically very stable with no measurable degradation during a 1500 h long operation at 700 °C and 0.5 A cm^{-2}. The power density of the ASC reached 0.79 W cm^{-2} at 750 °C at a cell voltage of 0.6 V. Impedance spectra recorded *in situ* during the test found no changes in the electrochemical behavior of the cell. Post test micro-structural investigation by SEM on the cathode side revealed no significant change in grain size and microstructure of the LSC infiltrate when compared to an untested counterpart fired at the same maximum temperature. The apparent stability of the anode supported cell with an LSC infiltrated-CGO cathode should provide a motivation to further explore the integration of a cathode prepared by infiltration into SOFC technology.

Acknowledgments

Appendix A. Supplementary data

Supplementary data related to this article can be found online at doi:10.1016/j.jpowsour.2012.05.040.

References

[1] S.P. Jiang, Int. J. Hydrogen Energy 37 (2012) 449–470.
[2] S.P. Jiang, Mater. Sci. Eng. A 418 (2006) 199–210.
[3] J.M. Vohs, R.J. Gorte, Adv. Mater. 21 (2009) 943–956.
[4] M. Shah, S.A. Barnett, Solid State Ionics 179 (2008) 2059–2064.
[5] F. Zhao, R. Peng, C. Xia, Mater. Res. Bull. 43 (2008) 370–376.
[6] A. Samson, M. Søgaard, R. Knibbe, N. Bonanos, J. Electrochem. Soc. 158 (2011) B650–B659.
[7] W. Wang, M.D. Gross, J.M. Vohs, R.J. Gorte, J. Electrochem. Soc. 154 (2007) B439–B445.
[8] T.Z. Sholklapper, V. Radmilovic, C.P. Jacobson, S.J. Visco, L.C. De Jonghe, Electrochem. Solid State Lett. 10 (2007) B74–B76.
[9] B. Dalslet, P. Blennow, P.V. Hendriksen, N. Bonanos, D. Lybye, M. Mogensen, J. Solid State Electrochem. 10 (2006) 547–561.
[10] S.C. Singhal, K. Kendall, Chapter 10: Testing of Electrodes, Cells, and Short Stacks, High Temperature Solid Oxide Fuel Cells: Fundamentals, Design, and Applications, Elsevier Ltd., Oxford, UK, 2003, p. 261.
[11] J.T.S. Irvine, J.W.L. Dobson, T. Politova, S. Garcia Martin, A. Shenouda, Faraday Discuss. 41 (2007) 41–49.
[12] A.V. Berenov, A. Atkinson, J.A. Kilner, E. Bucher, W. Sitte, Solid State Ionics 181 (2010) 819–826.
[13] P.S. Manning, J.D. Sirman, J.A. Kilner, Solid State Ionics 93 (1996) 125–132.
[14] J. Yang, H. Muroyama, T. Matsui, K. Eguchi, Int. J. Hydrogen Energy 35 (2010) 10505–10512.